

FRIDA: Fisheye Re-Identification Dataset with Annotations

Mertcan Cokbas, John Bolognino, Janusz Konrad, Prakash Ishwar*
 Department of Electrical and Computer Engineering, Boston University
 8 Saint Mary’s Street, Boston, MA 02215

[mcokbas, jcbolo, jkonrad, pi]@bu.edu

Abstract

Person re-identification (PRID) from side-mounted rectilinear-lens cameras is a well-studied problem. On the other hand, PRID from overhead fisheye cameras is new and largely unstudied, primarily due to the lack of suitable image datasets. To fill this void, we introduce the “Fish-eye Re-Identification Dataset with Annotations” (FRIDA)¹, with 240k+ bounding-box annotations of people, captured by 3 time-synchronized, ceiling-mounted fisheye cameras in a large indoor space. Due to a field-of-view overlap, PRID in this case differs from a typical PRID problem, which we discuss in depth. We also evaluate the performance of 10 state-of-the-art PRID algorithms on FRIDA. We show that for 6 CNN-based algorithms, training on FRIDA boosts the performance by up to 11.64% points in mAP compared to training on a common rectilinear-camera PRID dataset.

1. Introduction

Knowing the number and location of people in public spaces, office and school buildings, stores and shopping malls, etc., is critical for public safety (fire, chemical hazards), spatial analytics (optimization of office or store space usage), HVAC energy reduction, and, recently, for pandemic management. Typically, people-detection systems use standard surveillance cameras (equipped with rectilinear lens) mounted high on walls above the scene of interest. Since such cameras have a relatively narrow field of view (FOV), a number of them must be installed and managed which significantly increases the system complexity and cost, especially in large spaces.

Recently, overhead fisheye cameras have been successfully proposed for people counting [23, 17, 9]. However, even a fisheye camera with its large FOV cannot accurately detect people at the FOV periphery (large distance from the camera) due to extreme foreshortening and geometric dis-

tortions. Clearly, in such spaces (e.g., a convention hall) multiple overhead fisheye cameras are needed. However, since the same person may appear in FOVs of multiple cameras, person re-identification (PRID) is critical for accurate people counting, tracking, etc.

While PRID for *side-mounted, rectilinear-lens* cameras has been researched in depth [22, 6, 28, 31, 26, 27], we are aware of only three works exploring fisheye PRID [1, 2, 3], each with its own limitations and none releasing their fisheye data. Therefore, to inspire more research in this area, we are proposing a first-of-its-kind dataset, “Fisheye Re-Identification Dataset with Annotations” (FRIDA), that was captured by three overhead fisheye cameras in a large space and includes over 240,000 bounding-box annotations of people. In addition to introducing FRIDA, we explore its use for image-based PRID. An alternative use-case for FRIDA is as a video-dataset for tracking, but this is not the focus of our work.

Typical PRID datasets are not designed for people counting and were captured by side-mounted, rectilinear-lens cameras without FOV overlap. In this case, the goal is to identify the same person in two images captured by two cameras at *different* times. FRIDA, however, is meant for people counting and was captured by time-synchronized, overhead, fisheye cameras with *fully-overlapping* FOVs ($360^\circ \times 185^\circ$). In this case, the goal is to identify the same person in two images captured by two cameras at the *same* time. This explains the difference between the gallery sets of typical PRID datasets and FRIDA. In the former, for a given query there may be multiple ground-truth gallery elements, captured at different times. In FRIDA, for a given query there may be at most *one* gallery element at a given time instant. In case of occlusion, there is no gallery element for a given query (see Section 3 for details).

We also evaluate the performance of 10 state-of-the-art PRID methods on FRIDA: 6 methods developed for typical PRID datasets [22, 6, 26, 31, 28, 13] and 4 methods developed for overhead fisheye cameras [3]. The results show that training CNN-based methods on FRIDA (2-fold cross-validation) improves performance by 4.99-11.64% points in

*This work was supported by ARPA-E (agreement DE-AR0000944) and by Boston University Undergraduate Research Opportunities Program.

¹vip.bu.edu/frida

978-1-6654-6382-9/22/\$31.00 2022 IEEE

mAP compared to training on a typical PRID dataset [29].

The main contributions of this work are:

- We introduce a new PRID dataset, FRIDA, for indoor person re-identification using time-synchronized overhead fisheye cameras. This is the first overhead fisheye dataset for PRID and will be made publicly available.
- We evaluate the performance of 10 state-of-the-art PRID methods on FRIDA using two metrics. We compare the performance of 6 of those algorithms, when training on FRIDA against training on the non-fisheye Market-1501 dataset [29].

2. Related Work

2.1. Datasets

There exist several datasets for person re-identification using side-mounted rectilinear-lens cameras. Table 1 lists key statistics of the most common ones: VIPeR [11], PRID 2011 [14], Airport [15], CUHK03 [18], GRID [20], MSMT17 [25], Market-1501 [29] and iLIDS [30], but more details can be found in [27]. All these datasets have been designed with the goal of matching the image of a person from the query set to an image from the gallery set, and the query and gallery sets consist of images captured by *different* cameras. Moreover, different cameras have no field-of-view overlap so query and gallery images of the same identity have been captured at *different time instants*. Finally, in most of these datasets there are, typically, *multiple* gallery images having the same ID as the query image.

While there exist people-focused datasets captured by overhead fisheye-lens cameras (PIROPO [7], BOMNI [8], MW [21], HABBOF [17], CEPDOF [9], WEPDFOB [24]), they have been developed with the goal of people detection and, in some cases, tracking. However, each dataset only consists of frames from a *single* camera which severely limits the variability of body appearance, unlike in FRIDA.

Table 1. Commonly-used image datasets for person re-identification. (BBox = bounding box)

Dataset	Year	# BBoxes	# Cameras	Frame Resol.
VIPeR [11]	2007	1,264	2	Fixed
iLIDS [30]	2009	476	2	Variable
GRID [20]	2009	1,275	8	Variable
PRID 2011 [14]	2011	24,541	2	Fixed
CUHK03 [18]	2014	13,164	2	Variable
Market-1501 [29]	2015	32,668	6	Fixed
Airport [15]	2017	39,902	6	Fixed
MSMT17 [25]	2018	126,441	15	Variable
FRIDA	2022	242,809	3	Fixed

2.2. Algorithms

Person re-identification using rectilinear-lens cameras is a well-studied problem. Early approaches were model-

based [12, 10, 19, 16] and used hand-crafted features. Recent approaches use deep learning [22, 6, 5, 4, 28, 31, 26, 27] and outperform the traditional methods.

Sun *et al.* proposed PCB [22] in which feature vectors are uniformly partitioned in an intermediate layer to obtain part-informed features. This structure allows to separately focus on different parts of an image and extract local information for each part. Zheng *et al.* proposed a network called Pyramid [28] which does not only focus on part-informed local features, but also accounts for global features in addition to gradual cues. Pyramid achieves this through a coarse-to-fine model, which performs image matching by leveraging information from different spatial scales. Chen *et al.* proposed an attention-based network called ABD-Net [6], which instead of a small portion of an image focuses on its wider aspect by means of a diverse attention map. This is accomplished by combining two separate modules: one module focuses on context-wise relevance of pixels while the other module focuses on spatial relevance of these pixels. Zhu *et al.* proposed a network called VAREID [31] that allows matching of people regardless of the viewpoint from which they were captured. Instead of creating a separate space for each viewpoint (i.e., front, side, back), they create a unified hyperspace which accommodates viewpoints in-between the main viewpoints (e.g. side-front, side-back, etc.). Recently, Wieczorek *et al.* proposed a CTL model (Centroid Triplet Loss model) [26], which extends the triplet loss. When working with triplet loss, it is typical to choose one positive sample and one negative sample for an anchor. However, in the CTL model, instead of choosing a single sample, a centroid is computed over a set of samples which significantly improves performance.

The methods above have been designed for and tested on images from rectilinear-lens cameras. Very few PRID methods have been developed for overhead fisheye cameras. An early approach, proposed by Barman *et al.* [1], matches images of people who appear at the same radial distance from a camera (similar viewpoints). This is restrictive, and leads to sub-par performance, since people often appear at different distances from FOV centers in different cameras. Another algorithm proposed by Blott *et al.* [2] applies tracking to extract front-, back- and side-view images of a person. A person-descriptor is built by fusing features extracted from individual views. The algorithm does not perform PRID for each pose/viewpoint. Moreover, there is no guarantee that a person will appear at all 3 viewpoints during a recording, thus limiting performance. Recently, Bone *et al.* [3] proposed a PRID method for fisheye-lens cameras with overlapping FOVs. This approach leverages locations of people in images *instead* of their appearance. Using a calibrated fisheye-lens model this method maps pixel-location of a person in a query image to a pixel-location in a gallery image. The mapped query-person location is compared to

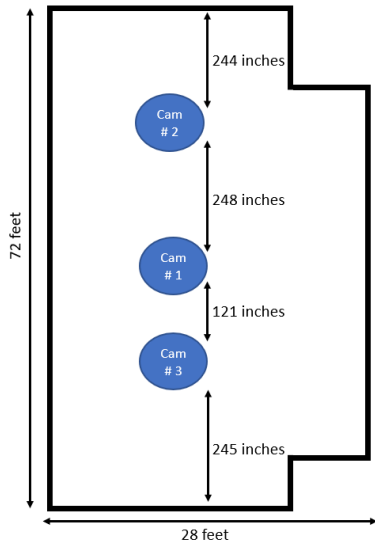


Figure 1. Bird's eye view of the space where FRIDA was collected.

locations of people in the gallery image to establish a match. The advantage of this algorithm is that it does not rely on a person's appearance, but it requires camera calibration (intrinsic parameters) and the knowledge of camera position in the 3D world (distance/rotation between cameras, mounting height). No datasets were published from these studies.

3. FRIDA Dataset

FRIDA is the first PRID dataset captured indoors by multiple overhead fisheye cameras and will be made publicly available². In FRIDA, the cameras have fully-overlapping FOVs ($360^\circ \times 185^\circ$), unlike in typical PRID datasets, and are time-synchronized (frames are captured at the same time). FRIDA was collected in a $2,000\text{ft}^2$ room using 3 ceiling-mounted fisheye cameras (100in above the ground). The bird's eye view of the room is shown in Fig. 1, and an example of time-synchronized frame triplet is shown in Fig. 2. The frames were captured by three Axis M3057-PLVE cameras at $2,048 \times 2,048$ -pixel resolution and 1.5 frames/sec. Annotations in FRIDA consist of 242,809 bounding boxes drawn around people (Table 1).

FRIDA can be used in a number of ways: as an image-based dataset for PRID, as a video-based dataset for people-tracking, or just for people detection and counting. In this paper, to demonstrate its most unique features, we treat it as an image-based PRID dataset. Below, we discuss the unique characteristics and challenges of FRIDA.

Annotations: At each time instant, three video frames are available with manually drawn, human-aligned bounding boxes for all people visible in each frame. Each bounding box is represented by 6 parameters: x, y, w, h, α, ID , where (x, y) are the coordinates of its center, (w, h) are its width and height, α is its counter-clockwise rotation angle with respect to the vertical axis of the image, and ID is the

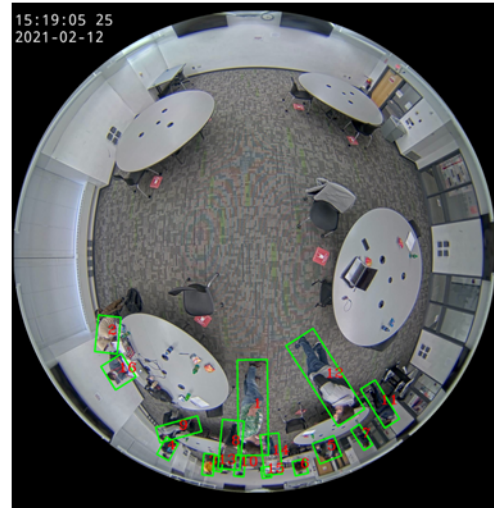


Figure 2. Example of three synchronously-captured fisheye images with annotations from FRIDA (top: camera 2, middle: camera 1, bottom: camera 3).

²vip.bu.edu/frida

Table 2. Detailed information about FRIDA (Fisheye Re-Identification Dataset with Annotations).

	# frames	# BBoxes	# BBoxes per frame	Scenarios/Challenges
Segment 1	7,017	66,810	3-15	People coming in and settling down; evenly distributed around the room; mostly sitting (lower bodies mostly occluded)
Segment 2	3,471	53,460	13-18	People walking around the room; significant occlusions
Segment 3	6,207	103,141	13-17	Concentration of people in parts of the room; people standing and staying close to each other; people strongly occluding each other
Segment 4	1,623	20,028	5-16	People leaving the room; occasional occlusions at entry/exit points

ID number of a person. Each person in the dataset is assigned a unique ID which is consistent in all frames of the dataset. There are 20 unique ID numbers in FRIDA.

Scenarios: FRIDA consists of four segments where each segment captures a different type of challenge (Table 2). In segment #1, people enter the room, walk and sit down (people are evenly distributed in the room). This segment resembles a lecture where people remain seated for most of the time and their lower bodies are mostly occluded. Segment #2 is the most crowded and dynamic segment. People are constantly moving which occasionally causes severe occlusions, especially when people are close to each other. This segment resembles a social meeting where people are wandering around the room and talking to each other. Segment #3 is the longest one and has over 100,000 bounding boxes. Participants gather at either end or in the middle of the room. They stand close to each other leading to severe occlusions. Segment #4 is the shortest, with people leaving the room and causing occasional occlusions at the doors.

Single sample of ID in the gallery set: In typical PRID datasets, for a given query element there are multiple samples in the gallery set with the query ID. In FRIDA, however, frames are captured at the same time instant and the identities in one frame are treated as the query set while identities in another frame are treated as the gallery set. Therefore, for a given query element there can be at most one sample with the query identity in the gallery set. In some cases, due to occlusions, a person may not be visible from a camera. This may lead to a no-match scenario at certain time instants for some query elements. Note that FRIDA can also be used for typical PRID by constructing the gallery from multiple images of the same ID captured at different times, but this is not in the scope of this work.

Synchronous, overhead capture: Due to the overhead placement of cameras and simultaneous capture, the viewpoint of a person directly under one camera may be dramatically different from the viewpoint from another camera. This is unlike in most other PRID datasets where it is common to capture a person from similar viewing angles (e.g., front, back, side, top) using different cameras. Then, if one of the gallery elements has the same viewpoint as the query, the chance of a match increases. However, in FRIDA, since the query and gallery elements are synchronously recorded

by different overhead cameras, people never appear from the same viewpoint. This can be seen in Fig. 2 where person #14 is seen from the top in camera #1 view, from the front in camera #3 view and from the back in camera #2 view. This makes the problem of PRID more challenging in FRIDA compared to other datasets.

Fisheye distortions: Since FRIDA has been recorded by fisheye cameras, images are subject to radial geometric distortions, especially close to FOV periphery. When a person is located at a different distance to each camera, the person’s appearance is geometrically distorted to a different degree in each camera view. This makes the problem of PRID more challenging in FRIDA compared to other datasets.

Resolution mismatch between query and gallery sets: The synchronous, overhead capture and fisheye distortions often lead to very differently-sized bounding boxes for the same person (resolution mismatch). Examples can be seen in Fig. 2, e.g., person #15 appears with very different resolutions in camera #2 and camera #3 views. In Fig. 3, we demonstrate this resolution mismatch quantitatively. The resolution ratio R between two bounding boxes B_1 and B_2 is defined as follows:

$$R = \frac{\min(\text{Area}(B_1), \text{Area}(B_2))}{\max(\text{Area}(B_1), \text{Area}(B_2))}. \tag{1}$$

Each data point in the plot shows the number of bounding-box pairs such that $R \leq \rho$ with $0 \leq \rho \leq 1$. Note that, the resolution mismatch is the largest (highest curve) between cameras 2 and 3 since they are farthest apart (Fig. 1).

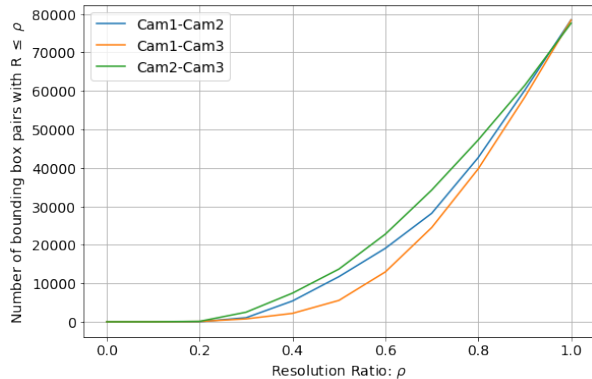


Figure 3. Bounding-box resolution mismatch for all camera pairs.

4. Experiments

4.1. Algorithms

In order to gauge challenges offered by FRIDA, we evaluated ten state-of-the-art PRID algorithms on it. Six of these algorithms: PCB [22], Pyramid [28], ABD-Net [6], VA-reID [31], CTL [26] and ResNet-50 [13], are CNN-based and use person’s appearance for re-identification. The remaining four algorithms are geometry-based and use person’s location in fisheye images for re-identification [3]. They differ in terms of the re-identification metric used: point-to-point distance (PPD), point-to-set total distance (PSTD), point-to-set minimum distance (PSMD) and count-based distance (CBD). FRIDA’s annotations serve as the input for all methods: bounding-box RGB values for appearance-based methods and bounding-box center for geometry-based methods. In each algorithm, we used hyper-parameters suggested in the corresponding paper.

4.2. Implementation Details

The testing procedure for all methods was the same. For a given pair of video frames, we treated all people from one frame as the query set (images or locations) and those from the other frame as the gallery set (images or locations).

In CNN-based methods, we fed the image of a person (within the person’s bounding box) into a network and extracted a feature vector from the final convolutional layer to serve as this image’s descriptor. We computed the cosine similarity between all normalized feature vectors of the query and gallery sets, resulting in a score matrix for each pair of frames³. We applied greedy matching to the score matrix to match the query and gallery elements as follows. We found the highest matching score, considered the corresponding elements to be a match and removed their row and column from the table. We repeated this process until no more removals were possible. We used this algorithm since in FRIDA the fisheye cameras have a fully-overlapping FOV and, therefore, a person can have at most *one* match in another camera’s FOV (and can be removed from the score matrix). This is different than testing on typical PRID datasets, where the matching of a given query does not affect the matching of other query elements.

In geometry-based algorithms, we first performed camera calibration as outlined in [3]. Using the calibrated camera model, each algorithm maps pixel locations of people (centers of bounding boxes) in the query frame (set) to pixel locations in the gallery frame (set). The matching is performed using different distance measures between the mapped query locations and gallery locations. Importantly, the geometric mapping depends on the height of a person [3]. In PPD, the mapping is performed for an average per-

son’s height (168cm) and the Euclidean distance from the mapped query location to a gallery location serves as the distance measure. In PSTD, query locations are mapped to the gallery frame for 21 different heights of a person (128-208cm). The *sum* of the Euclidean distances from 21 mapped query locations to a gallery location serves as the distance measure. The PSMD algorithm is very similar except that the *minimum* of 21 Euclidean distances instead of their sum is used as the distance measure. In CBD, again 21 mapped query locations are produced and the number of such locations that are closest to a gallery location is used to compute a distance measure. The distance measure computed in each case is used to construct a distance matrix for greedy matching as described above (except that the *smallest* distance is considered a match). Since so-defined distance measures are not symmetric, we performed bidirectional matching. For more details, see [3].

4.3. Dataset Splits

Despite more than 240,000 bounding boxes, FRIDA has only 20 different identities. Since this is insufficient for separate training, validation and testing sets, we evaluate the algorithms using 2-fold *identity-wise* cross-validation. We use half of the identities in training and the other half in testing, and then we swap the roles of identities and repeat the process. Specifically, we created the training set by choosing 50 random time stamps for each identity and taking 3 images (one from each camera) captured at this time (cameras are synchronized). This allowed a rich training set with many different viewpoints of the same person. We will provide the training sets we used as part of FRIDA. In the testing sets, we use *all* frames with the specific identities.

We also trained the CNN-based networks on Market-1501 [29] and tested them on FRIDA. Market-1501 is a commonly-used PRID dataset composed of images captured by side-view, rectilinear-lens cameras (different cameras capture a person at different times). For fairness, we used the same cross-validation testing sets as when both training and testing on FRIDA. We used the same testing sets for the geometry-based algorithms.

4.4. Evaluation Metrics

We use the *Query Matching Score* (QMS) [3] and *mean Average Precision* (mAP) as evaluation metrics. QMS is very similar to the commonly-used *Correct Matching Score* (CMS), and is defined as follows:

$$QMS = \frac{\sum_{n=1}^N \sum_{q \in Q_n} \mathbb{1}(q = \hat{q})}{\sum_{n=1}^N |Q_n \cap G_n|}$$

where N denotes the number of frames, Q_n, G_n are the sets of query and gallery identities in frame number n , respectively, and \hat{q} is the predicted identity of query q or “null” if there is no match. The important difference between QMS

³Since cosine distance is symmetric, it is not important which frame is chosen as the query set and which as the gallery set.

Table 3. Performance comparison of the appearance-based algorithms trained on **Market-1501** and tested on **FRIDA**. The highest values of QMS and mAP for each camera pair and for the cumulative are shown in boldface.

	QMS [%]				mAP [%]			
	C.1+C.2	C.1+C.3	C.2+C.3	Cumulative	C.1+C.2	C.1+C.3	C.2+C.3	Cumulative
ResNet-50 [13]	57.63	73.99	45.33	59.04	70.03	79.41	59.33	69.63
PCB [22]	56.63	74.64	45.62	59.02	70.91	79.28	59.79	70.04
ABD [6]	61.26	73.68	44.22	59.78	70.80	77.93	58.71	69.19
Pyramid [28]	74.58	84.66	54.88	71.46	78.72	86.38	64.89	76.72
VA-ReID [31]	60.79	74.18	44.99	60.06	71.21	78.68	59.31	69.78
CTL [26]	66.92	83.68	42.88	64.59	72.57	84.99	57.44	71.72

Table 4. Performance comparison of the appearance-based algorithms trained on **FRIDA** and tested on **FRIDA**. The highest values for QMS and mAP for each camera pair and for the cumulative are shown in boldface.

	QMS [%]				mAP [%]			
	C.1+C.2	C.1+C.3	C.2+C.3	Cumulative	C.1+C.2	C.1+C.3	C.2+C.3	Cumulative
ResNet-50 [13]	64.93	75.79	50.11	63.67	76.20	81.60	68.00	75.30
PCB [22]	63.30	74.79	51.77	63.33	75.79	81.23	67.91	75.01
ABD [6]	75.31	83.18	62.05	73.57	82.43	85.16	74.81	80.83
Pyramid [28]	67.79	80.78	53.48	67.42	75.38	81.59	68.61	75.23
VA-ReID [31]	67.52	79.46	54.59	67.24	76.58	82.74	68.00	75.81
CTL [26]	77.30	90.11	64.76	77.44	82.7	89.79	75.17	82.58

and CMS is that QMS accounts for situations when there is no match between a query and gallery elements ($|Q_n \cap G_n|$ in the denominator). Basically, QMS gives the ratio of the number of correct matches to the number of true matches. We also compute the commonly-used mAP. It is important to note that in our scenario there exists *at most* one matching gallery-frame identity for a given query element. Unlike in classical PRID, we can encounter a query whose identity is absent from the gallery (due to complete occlusion). We exclude such cases from the mAP calculation.

4.5. Results

In Table 3, we report results for the six appearance-based CNN algorithms trained on Market-1501 and tested on FRIDA. In Table 4, we report results for the same algorithms, but both trained and tested on FRIDA. These results are computed over all 4 segments of FRIDA for each camera pair. We also report the cumulative QMS value which is computed as the total number of correct matches from all camera pairs and all segments divided by the total number of possible correct matches from all camera pairs and all segments. In addition to QMS, we report mAP (the cumulative mAP is computed in a manner analogous to cumulative QMS). The common trend in both tables is that all algorithms achieve the highest QMS/mAP for cameras 1 and 3, and the lowest for cameras 2 and 3. This was to be expected since cameras 1 and 3 are the closest to each other (Fig. 1); people are captured at a more similar resolution, viewpoint and geometric distortion compared to other camera pairs. Conversely, the distance between cameras 2 and 3 is the largest which makes PRID more challenging.

As Table 3 shows, when trained on Market-1501, Pyramid [28] performs the best among the six appearance-based methods and outperforms the second-best algorithm, CTL [26], by 6.87% points in terms of cumulative QMS, and by 5.0% points in terms of cumulative mAP.

When these algorithms are trained on FRIDA (Table 4), CTL [26] outperforms other networks by 3.87-14.11% points in cumulative QMS and by 1.75-7.57% points in cumulative mAP. For cameras 1 and 3, CTL performs above 90% in terms of QMS. When trained on FRIDA, all networks achieve cumulative QMS above 63% and cumulative mAP above 75%.

Comparing the performance of algorithms trained on Market-1501 versus those trained on FRIDA, all the networks performed better when trained on FRIDA except for Pyramid. In terms of cumulative QMS, the improvement achieved by training ResNet-50, PCB, ABD, VA-ReID and CTL on FRIDA ranges from 4.31% to 13.79% points. In terms of cumulative mAP, these networks improve by 4.97% to 11.64% points by training on FRIDA. Considering the large number of bounding boxes in FRIDA, these margins correspond to thousands of correct matches between identities. It is impressive that training on Market-1501 using 750 identities and 9,928 bounding boxes is outperformed by training on FRIDA with only 10 identities and less than 1,500 bounding boxes. This suggests that for an effective PRID on overhead fisheye images, having a higher variability of the viewpoint (including overhead) for each identity is more important than having more identities with less viewpoint variability. We note, however, that Pyramid is an exception to this observation. This seems to suggest

Table 5. Performance comparison of the geometry-based algorithms [3] on FRIDA. The highest values for QMS and mAP for each algorithm are shown in boldface.

	QMS [%]					mAP [%]				
	Seg.1	Seg.2	Seg.3	Seg.4	Cumulative	Seg.1	Seg.2	Seg.3	Seg.4	Cumulative
PPD	99.51	87.39	80.60	90.77	88.02	99.49	94.47	90.13	93.95	93.93
PSMD	99.58	91.21	85.69	87.99	90.75	99.83	95.62	91.98	94.16	95.06
PSTD	99.69	88.08	81.79	91.03	88.76	99.60	94.69	90.22	94.19	94.06
CBD	99.17	92.18	89.81	93.69	93.11	99.69	96.82	95.41	96.51	96.97

that Pyramid is able to leverage a plurality of identities more effectively than viewpoint variability.

Table 5 shows the performance of the geometry-based PRID algorithms for each segment of FRIDA. Clearly, all 4 algorithms did extremely well on segment 1 in which people are spread out fairly uniformly in the room and are never very close to each other. On the other hand, in segment 3 people stand very close to each other posing difficulties for location-based matching, resulting in the lowest performance among all segments. As expected, the algorithm based on the PPD distance metric (single query location mapping using an average person’s height) achieves the lowest performance among the four algorithms. Algorithms using a range of person’s height perform better with the CBD-based algorithm achieving the best performance in terms of the cumulative QMS (93.11%) and cumulative mAP (96.97%). This is consistent with observations in [3].

For a fair comparison between appearance-based and geometry-based methods, we focus on the cumulative QMS and cumulative mAP values in Tables 3–5, computed over all FRIDA segments and accumulated over all camera pairs. It is clear that each geometry-based algorithm outperforms all appearance-based methods by a huge margin. However, it should be noted that in geometry-based algorithms a careful calibration must be performed once for each camera model (intrinsic parameters) prior to deployment. During installation cameras must be level-mounted and their extrinsic parameters (camera installation height, distance and rotation between cameras) must be measured or calibrated, a process known as system commissioning. Since this information may not be available in some scenarios, geometry-based algorithms would not be applicable in those cases. On the other hand, the appearance-based methods do not require any information about room setup and are easier to deploy in new scenarios.

5. Conclusions

We introduced FRIDA, the first image dataset for person re-identification from overhead fisheye cameras. The dataset is unique not only for the camera type used but also for their overlapping fields of views that is often encountered when counting people in large spaces. This leads to a new type of PRID - matching of people “seen” by different cameras at the same time.

We evaluated the performance of 10 state-of-the-art PRID algorithms on FRIDA. Six of these algorithms were CNN appearance-based methods while four algorithms were based on geometry. The geometry-based algorithms performed significantly better than the appearance-based methods. The best-performing geometry-based method reaches almost 97% in cumulative mAP, computed across all dataset segments and camera pairs. This is close to a perfect re-identification. Only in high-density scenarios (people close to each other causing severe occlusions), does its performance drop to about 95%. However, geometry-based algorithms require calibration of each camera type used and additional measurements for each camera layout.

The appearance-based methods do not perform quite as well, even when trained on FRIDA, with the best one achieving below 83% in cumulative mAP. This suggests there is much space for improvement in appearance-based methods. On the other hand, they require no calibration or measurements, and can be applied “out of the box”.

We demonstrated that training CNN-based PRID methods on fisheye images improves performance when testing on fisheye images, which is not surprising. However, more research is needed to achieve *reliable* fisheye PRID in challenging scenarios (occlusions, high density of people). We hope FRIDA will inspire more research in this direction, and also serve as a benchmark for people detection, tracking and video-based PRID studies based on overhead fisheye cameras.

References

- [1] A. Barman, W. Wu, R. P. Loe, and A. M. Burry. Person re-identification using overhead view fisheye lens cameras. In *2018 IEEE International Symposium on Technologies for Homeland Security (HST)*, pages 1–7, 2018. 1, 2
- [2] G. Blott, J. Yu, and C. Heipke. Multi-view person re-identification in a fisheye camera network with different viewing directions. *ISPRS J. Photogrammetry, Remote Sensing and Geoinformation Science*, 87:263 – 274, 2019. 1, 2
- [3] J. Bone, M. Cokbas, O. Tezcan, J. Konrad, and P. Ishwar. Geometry-based person reidentification in fisheye stereo. In *17th IEEE International Conference on Advanced Video and Signal Based Surveillance (AVSS)*, 2021. 1, 2, 5, 7
- [4] B. Bryan, Y. Gong, Y. Zhang, and C. Poellabauer. Second-order non-local attention networks for person re-identification. In *2019 IEEE/CVF International Conference on Computer Vision (ICCV)*, pages 3759–3768, 2019. 2

- [5] G. Chen, C. Lin, L. Ren, J. Lu, and J. Zhou. Self-critical attention learning for person re-identification. In *2019 IEEE/CVF International Conference on Computer Vision (ICCV)*, pages 9636–9645, 2019. [2](#)
- [6] T. Chen, S. Ding, J. Xie, Y. Yuan, W. Chen, Y. Yang, Z. Ren, and Z. Wang. Abd-net: Attentive but diverse person re-identification. In *IEEE/CVF International Conference on Computer Vision (ICCV)*, pages 8350–8360, 2019. [1](#), [2](#), [5](#), [6](#)
- [7] C. R. del Blanco, P. Carballeira, F. Jaureguizar, and N. García. Robust people indoor localization with omnidirectional cameras using a grid of spatial-aware classifiers. *Signal Processing: Image Communication*, 93, 2021. [2](#)
- [8] B. E. Demiroz, I. Ari, O. Eroglu, A. A. Salah, and L. Akarun. Feature-based tracking on a multi-omnidirectional camera dataset. In *5th International Symposium on Communications, Control and Signal Processing*, pages 1–5, 2012. [2](#)
- [9] Z. Duan, M. Ozan T., H. Nakamura, P. Ishwar, and J. Konrad. Rapid: Rotation-aware people detection in overhead fisheye images. In *2020 IEEE/CVF Conference on Computer Vision and Pattern Recognition Workshops (CVPRW)*, pages 2700–2709, 2020. [1](#), [2](#)
- [10] M. Farenzena, L. Bazzani, A. Perina, V. Murino, and M. Cristani. Person re-identification by symmetry-driven accumulation of local features. In *2010 IEEE Computer Society Conference on Computer Vision and Pattern Recognition*, pages 2360–2367, 2010. [2](#)
- [11] D. Gray and H. Tao. Viewpoint invariant pedestrian recognition with an ensemble of localized features. In *Proceedings of the 10th European Conference on Computer Vision: Part I, ECCV '08*, page 262275, Berlin, Heidelberg, 2008. Springer-Verlag. [2](#)
- [12] D. Gray and H. Tao. Viewpoint invariant pedestrian recognition with an ensemble of localized features. volume 5302, pages 262–275, 10 2008. [2](#)
- [13] K. He, X. Zhang, S. Ren, and J. Sun. Deep residual learning for image recognition. In *2016 IEEE Conference on Computer Vision and Pattern Recognition (CVPR)*, pages 770–778, 2016. [1](#), [5](#), [6](#)
- [14] M. Hirzer, C. Beleznaï, P. M. Roth, and H. Bischof. Person re-identification by descriptive and discriminative classification. In *Proceedings of the 17th Scandinavian Conference on Image Analysis, SCIA'11*, pages 91–102, Berlin, Heidelberg, 2011. Springer-Verlag. [2](#)
- [15] S. Karanam, M. Gou, Z. Wu, A. Rates-Borras, O. Camps, and R. J. Radke. A systematic evaluation and benchmark for person re-identification: Features, metrics, and datasets. *IEEE Transactions on Pattern Analysis and Machine Intelligence*, 41(3):523–536, 2019. [2](#)
- [16] M. Kostinger, M. Hirzer, P. Wohlhart, P. M. Roth, and H. Bischof. Large scale metric learning from equivalence constraints. In *2012 IEEE Conference on Computer Vision and Pattern Recognition*, pages 2288–2295, 2012. [2](#)
- [17] S. Li, M. O. Tezcan, P. Ishwar, and J. Konrad. Supervised people counting using an overhead fisheye camera. In *2019 16th IEEE International Conference on Advanced Video and Signal Based Surveillance (AVSS)*, pages 1–8, 2019. [1](#), [2](#)
- [18] W. Li, R. Zhao, T. Xiao, and X. Wang. Deepreid: Deep filter pairing neural network for person re-identification. In *2014 IEEE Conference on Computer Vision and Pattern Recognition*, pages 152–159, 2014. [2](#)
- [19] S. Liao, Y. Hu, X. Zhu, and S. Z. Li. Person re-identification by local maximal occurrence representation and metric learning. In *2015 IEEE Conference on Computer Vision and Pattern Recognition (CVPR)*, pages 2197–2206, 2015. [2](#)
- [20] C. C. Loy, C. Liu, and S. Gong. Person re-identification by manifold ranking. In *2013 IEEE International Conference on Image Processing*, pages 3567–3571, 2013. [2](#)
- [21] N. Ma, R. B. Knapp, N. F. Polys, J.-B. Huang, A. Ibrahim, C. Hurt, and Y. Xiao. Mirror worlds challenge. www2.icat.vt.edu/mirrorworlds/challenge/index.html, 2018. [2](#)
- [22] Y. Sun, L. Zheng, Y. Yang, Q. Tian, and S. Wang. Beyond part models: Person retrieval with refined part pooling (and a strong convolutional baseline). In V. Ferrari, M. Hebert, C. Sminchisescu, and Y. Weiss, editors, *Computer Vision – ECCV 2018*, pages 501–518, Cham, 2018. Springer International Publishing. [1](#), [2](#), [5](#), [6](#)
- [23] M. Tamura, S. Horiguchi, and T. Murakami. Omnidirectional pedestrian detection by rotation invariant training. In *2019 IEEE Winter Conference on Applications of Computer Vision (WACV)*, pages 1989–1998, 2019. [1](#)
- [24] M. O. Tezcan, Z. Duan, M. Cokbas, P. Ishwar, and J. Konrad. Wepdtot: A dataset and benchmark algorithms for in-the-wild people detection and tracking from overhead fisheye cameras. In *IEEE/CVF Winter Conference on Applications of Computer Vision (WACV)*, pages 1381–1390, 2022. [2](#)
- [25] L. Wei, S. Zhang, W. Gao, and Q. Tian. Person transfer gan to bridge domain gap for person re-identification. In *2018 IEEE/CVF Conference on Computer Vision and Pattern Recognition*, pages 79–88, 2018. [2](#)
- [26] M. Wiczcerek, B. Rychalska, and J. Dabrowski. On the unreasonable effectiveness of centroids in image retrieval, 2021. [1](#), [2](#), [5](#), [6](#)
- [27] M. Ye, J. Shen, G. Lin, T. Xiang, L. Shao, and S. C. Hoi. Deep learning for person re-identification: A survey and outlook. *IEEE Transactions on Pattern Analysis and Machine Intelligence*, 2021. [1](#), [2](#)
- [28] F. Zheng, C. Deng, X. Sun, X. Jiang, X. Guo, Z. Yu, F. Huang, and R. Ji. Pyramidal person re-identification via multi-loss dynamic training. In *2019 IEEE/CVF Conference on Computer Vision and Pattern Recognition (CVPR)*, pages 8506–8514, 2019. [1](#), [2](#), [5](#), [6](#)
- [29] L. Zheng, L. Shen, L. Tian, S. Wang, J. Wang, and Q. Tian. Scalable person re-identification: A benchmark. In *2015 IEEE International Conference on Computer Vision (ICCV)*, pages 1116–1124, 2015. [2](#), [5](#)
- [30] W. Zheng, S. Gong, and T. Xiang. Associating groups of people. In *BMVC*, 2009. [2](#)
- [31] Z. Zhihui, X. Jiang, F. Zheng, X. Guo, F. Huang, X. Sun, and W. Zheng. Viewpoint-aware loss with angular regularization for person re-identification. *Proceedings of the AAAI Conference on Artificial Intelligence*, 34:13114–13121, 04 2020. [1](#), [2](#), [5](#), [6](#)